NOTICE CONCERNING COPYRIGHT RESTRICTIONS

Source Characteristics of Micro-Earthquakes at the Northwest Geysers Geothermal Field, California

Gisela Viegas and Lawrence Hutchings

Lawrence Berkeley National Lab

Keywords

Geysers, micro-earthquakes, induced seismicity, earthquake source, stress drop, radiated energy, Empirical Green's function

ABSTRACT

We investigate the source parameters of micro-earthquakes (<M3) at the Northwest Geysers, near an injection well, before and during water injection, looking for temporal and spatial variations. Our objective is to understand the relation among injection, production and source mechanisms of micro-earthquakes. To determine the source parameters of the micro-earthquakes, such as fault radius, stress drop, seismic moment and radiated energy, we use two techniques: the Empirical Green's Function (EGF) method; and the NetMoment method, and compare the source parameters results of micro-earthquakes used in both studies. Our results indicate that micro-earthquakes at the Northwest Geysers have on average small radius and large stress drops (median of 27.7 MPa). The stress drops of these induced micro-earthquakes are comparable to the ones of deeper, large (>M5.5), natural occurring tectonic earthquakes. Possible explanations for the high stress drop are, for example, fault re-strengthening by geochemical alteration or the fracturing of intact rock induced by the injection of cold water. This source information has implications for understanding the physics of faulting and for seismic potential assessment in areas of ongoing geothermal exploration.

Introduction

We investigate the source mechanisms of micro-earthquakes at the Northwest Geysers geothermal field in California between 2006 and 2010. Our objective is to understand the relation among injection, production and source mechanisms of micro-earthquakes. The injection of water into the ground has become a common procedure in the management of geothermal reservoirs. At The Geysers, which is a vapor dominated reservoir, the injection of water has improved productivity of the reservoir and extended the lifespan of an economically viable energy production activity. Water injection helps maintain the reservoir pressures and the flow rates at production wells, and improves the chemical quality of the steam. (Majer and Peterson, 2007a). However, the injection of water also produces an increase in micro-seismicity. The relationship between water injection and increased micro-seismicity at the Geysers has been established in many studies (e.g. Eberrhart-Phillips and Openheimer, 1986; Smith *et al*., 2000), showing a good correlation between the injection flux and the rate of increased micro-seismicity. Micro-seismicity is used as a tool in exploration management, as it can be used to track the release of strain and the injected fluid flow paths, and to characterize the permeability of the reservoir. However, the level of increased micro-seismicity has generated concerns among the nearby communities. The mechanism by which the micro-seismicity is triggered is not clear, and several possible mechanisms are considered. The presence of fluids perturbs the stress field (by changing the pore pressure) and/or facilitates chemical reactions that alter the frictional properties of the reservoir (by, for example, the precipitation of cements that bonds fracture walls; e.g., Karner, 2005). The injection of cold water into the reservoir may activate the thermal contraction of the rock either on pre-existing fractures, facilitating the slip, or generating new fractures (Majer and Paterson, 2007a). Poroelastic stressing is proposed as a production induced mechanism due to the reservoir contraction by the extraction of steam. Source information of both induced and tectonic micro-earthquakes at The Geysers will help constrain the possible mechanisms of the induced micro-seismicity, allowing for a more efficient reservoir management and a more realistic seismic potencial assessment. In this study, we estimate the source parameters of the Northwest Geysers micro-earthquakes that occurred between 2006 and 2010, looking for temporal and spatial variations. We also investigate how micro-seismicity evolves within a smaller crustal volume inside our study area, which surrounds an injection well. We estimate the source parameters of micro-earthquakes which occurred before and after the onset of water injection and look for possible temporal changes (November 2007).

To determine the source parameters of the micro-earthquakes, such as fault radius, stress drop, seismic moment and radiated en-

ergy, we use two techniques. One method is the Empirical Green's Function (EGF) method and the other method is the NetMoment method which simultaneously inverts for micro-earthquake source properties and medium attenuation. The EGF method has been proved to be a very efficient method for extracting the source information of small earthquakes (Viegas *et al*., 2010). It is a particularly good method to use when studying micro-earthquakes that occur in media that heavily attenuate seismic waves such as The Geysers, as it empirically corrects for attenuation and site effects. The NetMoment method is good when dealing with a large number of micro-earthquakes, as it simultaneously inverts for the source parameters of these micro-earthquakes (Gok *et al*., 2009), but carries larger uncertainties in the attenuation correction. The EGF method requires the use of an earthquake pair - a larger micro-earthquake and a smaller micro-earthquake which will act as a medium transfer function. The method further constrains that the smaller micro-earthquake, or the EGF micro-earthquake, needs to be collocated with the large micro-earthquake and have the same focal mechanism. These constrains on the EGF micro-earthquake severely limits the number of micro-earthquakes that can be analyzed, as a suitable EGF micro-earthquake may not be available. In this study, we use the source parameters estimates obtained with the EGF approach of a small number of micro-earthquakes, to validate and further constrain the source parameters of a larger dataset obtained with the NetMoment method. The EGF method can also be used to identify the fault plane orientation when source directivity is observed. Our goal is to characterize the source characteristics of the tectonic and induced micro-earthquakes at The Geysers and to understand how local stresses change as a result of water injection and steam extraction, the most common activities in geothermal energy production.

Data

We use micro-earthquakes recorded by the Lawrence Berkeley National Laboratory (LBNL) seismic array. The array consists of thirty 3-component short-period stations which continually telemeter digital data sampled at 500 samples per second to a central acquisition computer (Majer *et al*., 2007a). The seismic array has been continually recording data since the end of 2003, with the configuration varying somewhat over the years as new stations where added to the initial number of 23 stations (see Majer *et al*. (2007a) for a more detailed initial configuration of the seismic array). Figure 1 shows the current station distribution over The Geysers field. The good correlation between water injection and steam production with increased seismicity is well documented at The Geysers (e.g. Eberrhart-Phillips and Openheimer, 1986; Smith *et al*., 2000). In 2003, wastewater from Santa Rosa, CA, started to be directly injected through a pipeline, with an initial average flux of 41 million liters per day (Majer *et al*., 2007a). As a result of the geothermal development at The Geysers, the micro-seismic activity is significant, with more than 19,000 micro-earthquakes reported in 2006, 99% of which with magnitudes smaller than M2 (Majer *et al*., 2007b). From this huge dataset we select two subsets of data based on our goal to understand the relation between injection, production and induced micro-seismicity. One subset is selected to characterize micro-earthquakes which occur in a certain region before and during water injection. Here, we are looking for possible time variations in the micro-earthquakes source properties. The other subset is designed to characterize the sources of earthquake that occur throughout the Northwest Geysers region. This subset focuses on the largest earthquakes (>=M3), and we are looking for both spatial and temporal variability. For the first subset, we select the events that fall within a rectangular area surrounding the injection well Prati 9, since the beginning of 2006 until June 2010 (the time in which this study started). The injection of water on well Prati9 started in November 2007, and soon after an increase in micro-seismicity was observed and is ongoing at the time of this study. The boundaries of the rectangular area were selected in such a way that the study area includes most of the micro-earthquakes induced by water injection on well Prati9. The box has longitude and latitude coordinates of 122.8415 W, 122.8215 W, 38.8485 N and 38.8300 N, respectively. Figure 2 shows the yearly spatial distribution of micro-seismicity at the Northwest Geysers in a region surrounding the injection well Prati 9, from 2006 to April 2010. Also shown in Figure 2 is the location of the injection well Prati 31, which is scheduled to start injection in August 2010. Future work will include characterizing of the micro-seismicity induced by injection on well Prati 31. For the second subset, we select all >M3 earthquakes within a larger study area, and all smaller micro-earthquakes located within 100 meters of the >M3 earthquakes, which can be used as possible Empirical Green's Function events. We repeat the procedure for a comparable number of M2 micro-earthquakes, to obtain a good magnitude sampling. Figure 3 shows the location of all M3 earthquakes that occurred between January and April of 2010 at The Geysers and within our larger study area. Also shown in Figure 3 is the location of the injection well Prati 31, which is scheduled to start injection in August 2010. Future work will include characterizing of the micro-seismicity induced by injection on well Prati 31.

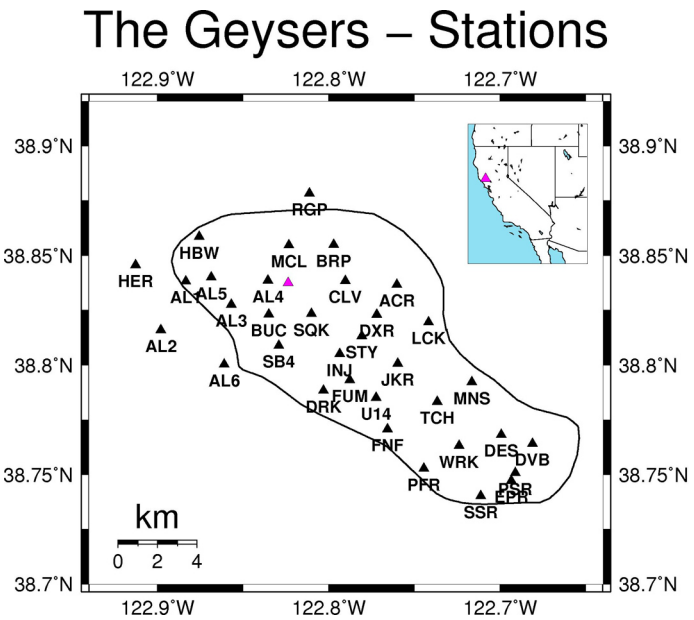

Figure 1. Station location map and boundary outline of the The Geysers geothermal field. The injection well Prati 9 (purple triangle) is shown for reference in both The Geysers area and the regional map on the inset.

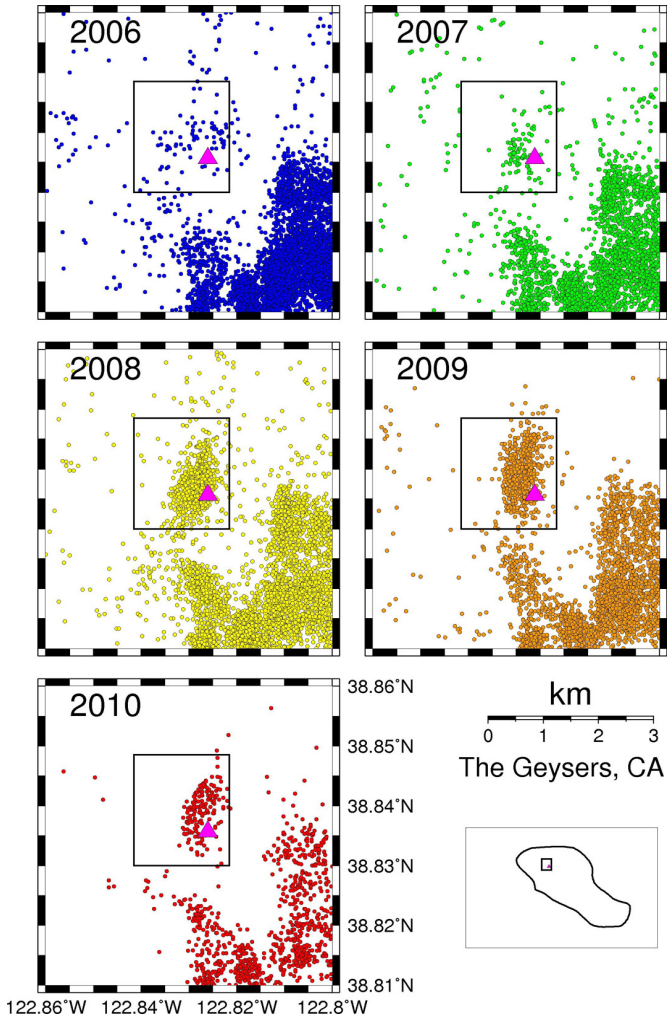

Figure 2. Spatial distribution of the micro-seismicity at the Northwest Geysers in a region surrounding the injection well Prati 9 (purple triangle), by year, from January 2006 to April 2010.

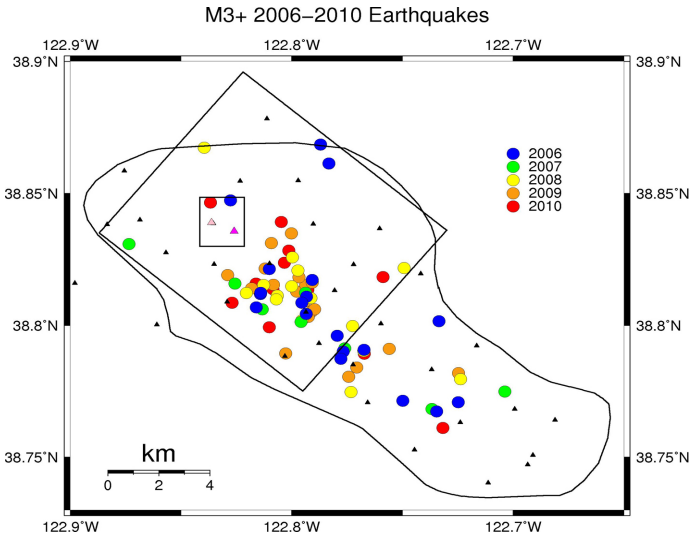

Figure 3. Location of all M3+ Geysers earthquakes which occurred since January 2006. The region surrounding the injection wells Prati 9 (purple triangle) and Prati 31 (pink triangle) is also shown. The larger square delimitates our study area at the northwest region of The Geysers.

Methods

To investigate the source characteristics of the micro-earthquakes at The Geysers, such as fault radius, stress drop, seismic moment and radiated energy, we use two methods: the Empirical Green's Function (Mori and Frankel, 1990; Hutchings and Wu, 1990); and the NetMoment method (Hutchings, 2002). We use the EGF method to validate the results of the NetMoment method by comparing the source parameters results of micro-earthquakes used in both studies. As stated before, the EGF method is particularly good at correcting for attenuation and site effects, but it is limited in the number of micro-earthquakes it can be applied to, whereas the NetMoment method is suitable for large datasets, but carries large uncertainties in the attenuation correction.

Empirical Green's Function Method

We obtain micro-earthquake source parameters using the Empirical Green's Function (EGF). The first step consists in forming micro-earthquake pairs. To do so, we first select the largest micro-earthquakes in our dataset. We then select smaller micro-earthquakes located within a radius of 100 meters of the largest micro-earthquakes. From these, we visually inspect for waveform similarity between the micro-earthquakes at all common recording stations. Similar travel paths and source mechanism translates into similar waveforms. We select the small micro-earthquake more similar with the large one as the EGF micro-earthquake, giving preference to micro-earthquakes which occurred closer in time, to avoid introducing uncertainties in the Green's function from temporal changes in the local stress field due to geothermal development activities, such as water injection and steam extraction. Once we select the micro-earthquake pair, we apply the EGF method in the frequency domain, following Abercrombie and Rice (2005). We use a multitaper approach developed by Prieto *et al.* (2009) which calculates the complex frequency spectrum of the micro-earthquakes, performs the complex spectral division, and transform back to time, to obtain the relative micro-earthquake source time function. A clear source pulse indicates the EGF is good in both amplitude and phase, validating our selection of the EGF micro-earthquake. Multitaper methods are more effective in preventing spectral leakage and preserving the spectral shape than standard individual taper methods, such as the cosine or Hanning taper method (e.g. Park *et al.*, 1987; Thomson, 1982). We analyze both P and S waves using the three-component instrument-corrected velocity-seismograms, when possible. The P wave signal usually has a lower signal to noise ratio than S wave signal and is more affected from a possible volumetric change at the source, frequently observed in micro-earthquakes in geothermal areas (e.g., Miller *et al.*, 1998; Console and Rosini, 1998; and Taggart *et al.*, 2007). Possible different volumetric changes will add uncertainty in the EGF micro-earthquake deconvolution. We use time windows of 0.4 seconds to calculate the spectra, starting 0.04 seconds before the P or S wave onset, long enough to record a complete direct wave of M4 and lower earthquakes. Time window length tests (e.g. Ide *et al.*, 2003; Sonley and Abercrombie, 2007) have shown that amplitude spectra are stable over a wide range of lengths above a certain minimum that contains the complete direct wave.

We use the same length window duration on the pre-P part of the seismogram for the noise data. We calculate the ratio between the complex spectrum of the two micro-earthquakes using the multi-tapering technique with a time-bandwidth product of 4, and 7 Slepian tapers. We model the amplitude spectral ratio (Ω_r) to obtain corner frequencies for the large (f_{c1}) and small (f_{c2}) micro-earthquakes, and the relative long period level of the ratio between the two micro-earthquakes (Ω_{0r}) using (Abercrombie and Rice, 2005),

$$\Omega_r(f) = \Omega_{0r}\left[\frac{1+\left(\frac{f}{fc_2}\right)^{\gamma n}}{1+\left(\frac{f}{fc_1}\right)^{\gamma n}}\right]^{\frac{1}{\gamma}}, \quad (1)$$

where f is the frequency, and γ and n are constants (γ = n = 2). γ controls the shape of the spectrum curvature around the corner frequency and n controls the high frequency fall off. We fit the spectral ratio in the bandwidth for which the signal is above the noise by a factor of 3 for both micro-earthquakes in the EGF pair. In the example of Figure 4 we deconvolve a magnitude 1.66 micro-earthquake from a magnitude 2.7 micro-earthquake. Both micro-earthquakes occurred in 2010 inside the box area defined around the injection well Prati 9 at a depth of 3 km.

NetMoment Method

Prior to the inversion, we correct the Fourier amplitude spectra of the recorded seismograms for average radiation pattern and geometrical spreading. We then scale the spectra to represent moment at the long-period asymptote. Following Aki and Richards (1980, p. 116), we correct the spectra by:

$$\Omega(f)_i = \frac{4\pi\rho_x^{1/2}\rho_\xi^{1/2}\beta_x^{1/2}\beta_\xi^{5/2}R^\alpha}{S^S F^S}U(f), \quad (2)$$

where $U(f)$ is the recorded displacement spectra at the station, ρ_χ is density at the station and ρ_ξ is density at the source, β_χ is shear velocity at the station and β_ξ is shear velocity at the source. S and F are the free surface correction and focal mechanism correction, respectively. Superscript s refers to values for S-waves discussed in Aki and Richards (1980, section 3.2). We use the P-wave velocity to obtain density (ρ) values following Lama and Vutukuri (1978). R^α is the geometrical spreading factor, where α = 1.0 for distances less than 100 km and 0.5 greater distances (Street *et al.*, 1975). Before analyzing the data, we rotate the seismograms into radial and transverse components. The focal mechanism radiation correction factor (F) is 0.47 for SV arrivals and 0.52 for SH arrivals. The free-surface correction factor (S) is obtained from the one-dimensional velocity model.

To solve for our free parameters, we use a nonlinear least-squares best fit of the Brune (1970) displacement spectral shape to the displacement spectra. We also allow a site-

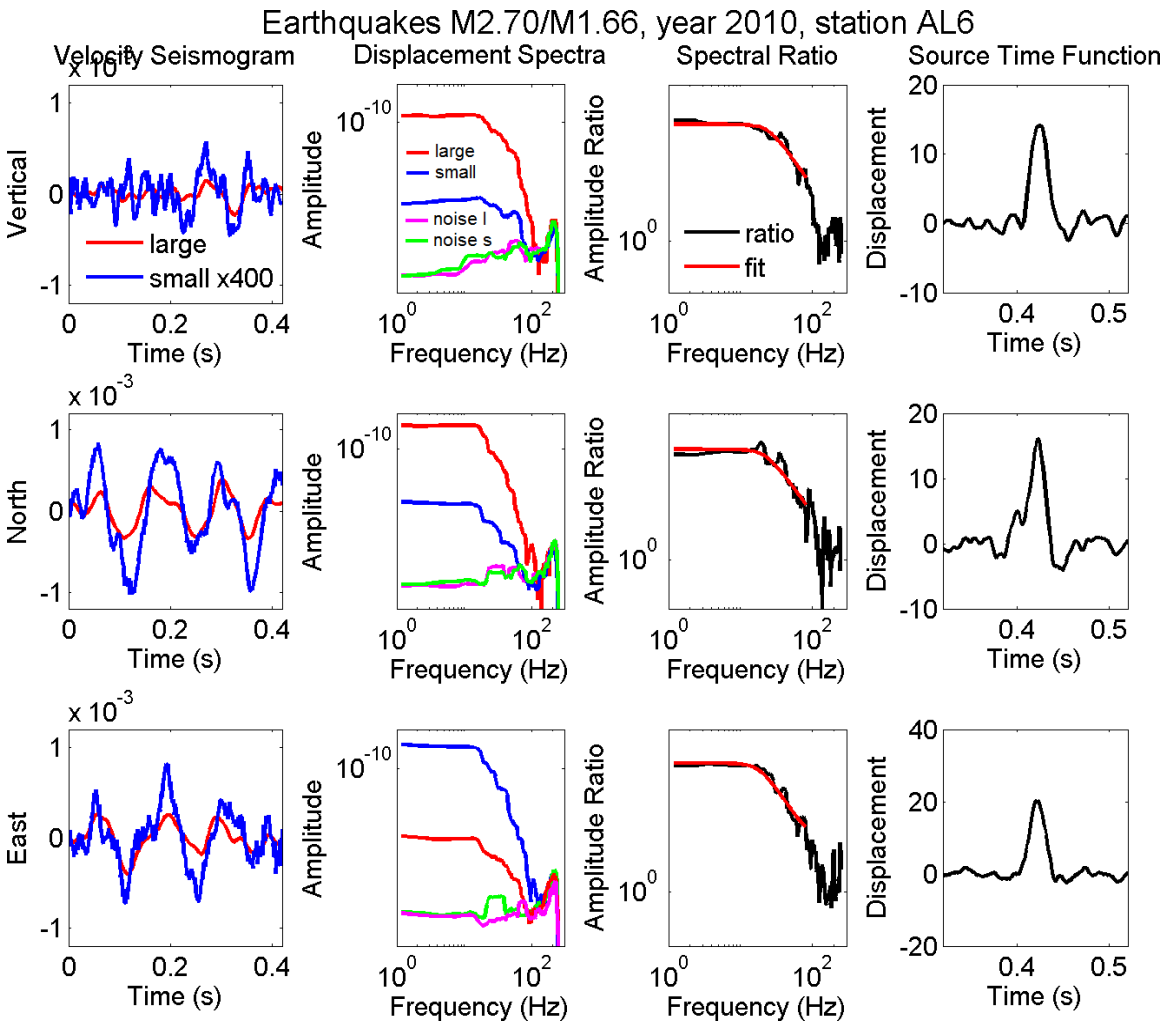

Figure 4. EGF method applied to a pair of 2010 Geysers micro-earthquakes (M2.7 and M1.7). We show for each component, from left to right, the overlay of the velocity seismograms of the two micro-earthquakes, the respective displacement spectra and noise spectra, the spectral ratio of the two micro-earthquakes and its model fit, and the relative source time function obtained by the deconvolution process. In this example, the corner frequency of the smaller micro-earthquake is outside the frequency band for which we have enough signal above noise.

specific attenuation operator. The corrected displacement spectra are fit to:

$$\Omega(f) = \frac{M_0 \exp(-\pi f k_i)}{\left[1+\left(\frac{f}{f_c}\right)^2\right]}, \quad (3)$$

where M_0 is the moment, f is frequency, f_c is the source corner frequency, κ_i is the combined site-specific and whole-path attenuation at station i. The best-fitting combination of free parameters (M_0, f_c, κ_i) is found by iteration from a starting model using the Simplex algorithm (Nelder and Mead, 1965; Caceci and Cacheris, 1984).

Source Parameters

Seismic Moment

We use the NetMoment method to calculate estimates the seismic moment of all the micro-earthquakes. The Magnitudes are estimated using the Hanks and Kanamori (1979) relationship.

Source Dimension and Stress Drop

We calculate the source dimension and the stress released by faulting from our corner frequency measurements. We use the magnitude (M_w) and seismic moment (M_0) values obtained from the NetMoment method. To calculate the fault radius, r, we use Madariaga's (1976) dynamic solution for a circular fault model,

$$r = \frac{k\beta}{f_c}, \quad (4)$$

where k is a constant (k = 0.32 for P waves and k = 0.21 for S waves) and β is the S wave velocity. We use depth-dependent P and S wave velocity estimates, based on the Romero *et al.* (1997) crustal model of The Geysers obtained using a 3D tomographic inversion.

The micro-earthquake source radius is determined by averaging the estimates at all available stations. At each station, the radius is calculated using the arithmetic mean of the corner frequencies of the available components of motion. We estimate the static stress drop ($\Delta\sigma$) from the seismic moment and source radius using Eshelby's (1957) circular static crack solution,

$$\Delta\sigma = \frac{7}{16}\frac{M_0}{r^3}. \quad (5)$$

Radiate Energy

We calculate the micro-earthquake radiated energy (E_S) for all the large micro-earthquakes in the EGF pairs. Energy estimates for all three components of P and S waves are determined following Boatwright and Fletcher (1984). We calculate the energy from a decade above and below the estimated micro-earthquake corner frequency to obtain at least 90% of the total radiated energy (Ide and Beroza, 2001). The total energy radiated by an micro-earthquake is calculated by summing the contributions of P and S wave energies (Ide *et al*., 2003) after we logarithmically average over all the stations the sum of the estimated energies at all the 3 components (Abercrombie 1995).

Results and Discussion

We present here our preliminary results from the analysis of 19 micro-earthquake which occurred inside the box surrounding the injection well Prati 9 (Table 1). Two of the micro-earthquakes occurred in 2006, before the injection of water started (November 2007), which we will call tectonic micro-earthquakes, and the remaining seventeen micro-earthquakes occurred in 2010, during injection, and will be designated by induced micro-earthquakes. The tectonic micro-earthquakes occurred at approximate depths of 1.7 and the induced ones of 3 km, except for the largest induced earthquake (M3) which was located at 0.03 km depth. We believe this location to be incorrect, and that the M3 earthquake occurred deeper. Figure 5 shows our seismic moment versus source radius preliminary results together with a global compilation of results from other studies, color coded by the method used or the data type. As can be seen in Figure 5, we obtain high average stress drops, comparable to and, for a few micro-earthquakes, slightly higher than deeper tectonic earthquakes. We obtain a median stress drop value of 27.8 MPa, well within the range of the expected stress drop of most large earthquakes (>M5.5) of 5.5 to 55 MPa (Kanamori, 1994), suggesting a similarity in the rupture process between small, induced micro-earthquakes and large, tectonic earthquakes. Three of the nineteen micro-earthquakes have stress drops higher than the lithostatic stress (81 MPa at 3 km depth assuming a rock density of 2700 kg/m^3), corresponding to the larger earthquakes in this dataset. High stress drop values are not unheard of in earthquake source studies. For example, very high stress drops (80 to >1000 MPa) were observed for moderate earthquakes (M4-M6) in Western US (Kanamori, 1994); Kim and Dreger (2008) found extremely high stress drops for asperities of the M6 2004 Parkfield earthquake using a slip inversion method; Imanishi and Ellsworth (2006) found very high stress drops (some > 100 MPa) for small earthquakes on the Parkfield segment of the San Andreas Fault, CA, recorded in the SAFOD main hole, using an EGF method; and Viegas *et al*. (2010) found extremely high stress drops (median 100 MPa) for a sequence of M5-M2 intraplate earthquakes in NY. High stress drop were also found for induced earthquakes. Tomic and Abercrombie (2009) found very high stress drops (between 26 MPa and 179MPa) for micro (M 2.1) shallow (<5km) reservoir induced earthquakes at the Açu Dam in Brazil, using an EGF method. Yamada *et al*. (2007) found stress drops of micro-earthquakes induced by the mining activity at a South African gold mine, to be comparable to the stress drop of naturally occurring tectonic earthquakes. Hough *et al*. (1999), using a multiple empirical Green's function approach, found that the stress drops (5.5 MPa to 110 MPa) of 61 shallow (<5 km) micro-earthquakes (M0 to M1.5) occurring at the Coso Geothermal Area, CA, were comparable to moderate tectonic earthquakes. Some of the first source studies of induced micro-earthquakes (either by mining or by hydraulic fracturing) gave estimated stress drops lower than those of tectonic earthquakes (e.g. see Gibowitz *et al*., 1991 (URL); and Fehler and Phillips, 1991 (Fenton Hill) results on Figure 4). These low stress drop results may be related with the methods used to retrieve the source parameters, which are not sufficiently correcting for attenuation. Tomic and Abercrombie (2009) and Yamada *et al*. (2007) study earthquakes in intraplate settings, where attenuation is lower. Hough *et al*. (1999) and Tomic and Abercrombie (2009) used an EGF method, more suitable for

Table 1. Identification and source parameters of the micro-earthquakes analyzed in this study.

ID	M_w	M_0 (Nm)	f_{cP} (Hz)	f_{cS} (Hz)	r (m)	$\Delta\sigma$ (Pa)	Depth (km)	ID EGF	M_w EGF
06132103830	3.46	1.88E+14	-	10.53	47.01	7.94E+08	1.53	06132161902	0.85
06134050010	2.08	1.66E+12	-	17.36	28.50	3.14E+07	1.87	06133231156	0.58
10012011213	2.64	1.13E+13	-	9.82	62.25	2.05E+07	3.68	06135182511	1.27
10107100929	2.70	1.77E+13	-	22.61	28.85	3.02E+07	3.40	10109025127	1.66
10008024122	1.90	9.62E+11	35.32	26.41	24.75	2.78E+07	3.17	10041020021	0.91
10018065517	1.88	8.39E+11	24.71	21.81	32.85	1.04E+07	3.26	10041095611	0.95
10035055603	2.29	3.60E+12	21.96	19.80	36.63	3.21E+07	3.31	10104073658	1.23
10036080504	2.26	3.00E+12	17.68	19.78	41.78	1.80E+07	3.44	10097033247	1.06
10037103254	2.06	1.53E+12	18.93	16.15	43.52	8.12E+06	3.27	10003120726	1.19
10043211305	2.49	6.90E+12	18.15	17.96	42.67	3.89E+07	3.81	10042060345	1.08
10047095224	2.14	1.93E+12	20.82	19.13	38.33	1.50E+07	3.25	10094013644	0.99
10049110344	2.12	2.03E+12	16.43	15.41	48.17	7.95E+06	3.63	10046131122	1.00
10052040338	2.22	2.75E+12	21.01	28.65	32.83	3.40E+07	3.37	09055195255	1.48
10096050733	2.39	5.75E+12	13.84	15.06	53.92	1.61E+07	3.55	10003120726	1.19
10097051937	1.80	7.66E+11	17.54	22.06	40.39	5.08E+06	3.11	10097033237	1.04
10109000805	2.32	4.38E+12	27.72	19.31	32.62	5.52E+07	3.41	10041095611	1.32
10109000812	2.14	2.58E+12	24.78	23.42	31.83	3.50E+07	3.46	10097033237	0.95
10109000901	2.00	1.46E+12	19.72	23.84	36.42	1.32E+07	3.13	10036081122	1.04
10117230711	3.08	6.79E+13	19.99	16.29	30.74	1.02E+09	0.03	08106144842	1.11

source studies of micro-earthquakes. Ide *et al*. (2003) found that the EGF method produced higher stress drop values than the typically used single event spectral analysis, as it empirically corrects for attenuation. Stress drop estimates in Figure 5 are color coded by method, with EGF methods in blue and various individual methods in light blue and light pink colors. All stress drop estimates with EGF methods are above 1 MPa. It seems that with increasing data quality and more accurate methods, stress drop estimates are getting higher. This is particularly apparent for micro-earthquakes (<M3).

The high stress drop values that we obtain may have several possible explanations. It may indicate that water injection may be inducing the fracturing of intact rock and not just facilitating the slip on pre-existing faults. Another possibility is that the existing fractures are being quickly strengthened above "normal" levels, promoted by the presence of fluids and the high temperature of the reservoir, which accelerates the fault healing rates through chemical processes, by lithification and densification of the rock from geochemical alteration which systematically fills crack like features, stiffening the rocks (Bonner *et al*., 2006). These are two among other possible mechanisms which can explain high stress drop values. The high crustal temperatures and the presence of fluids at The Geysers, may also change the stress conditions and the rock rheology of the reservoir, promoting alternative mechanisms of fault slip initiation. Once we include more data in our results, we will be able to better constrain our results. The high stress drop values that we obtain for the largest micro-earthquakes may be due to an higher uncertainties in the estimated valued. For example, the location of the M3 earthquake is not as accurate, and we may be overestimating the stress drop by using a slower wave velocity corresponding to the shallower crustal layers. A good EGF micro-earthquake is also harder to find for these larger, more complex micro-earthquakes.

Regarding the differences of source parameters between the micro-earthquakes which occurred pre and during water injection on the well Prati 9, our preliminary results show no differentiating trend, even though the possibly injection induced micro-earthquakes were slightly deeper, and higher stress drops could be expected. Again, once we include more micro-earthquakes in our study, a possible trend may be illuminated.

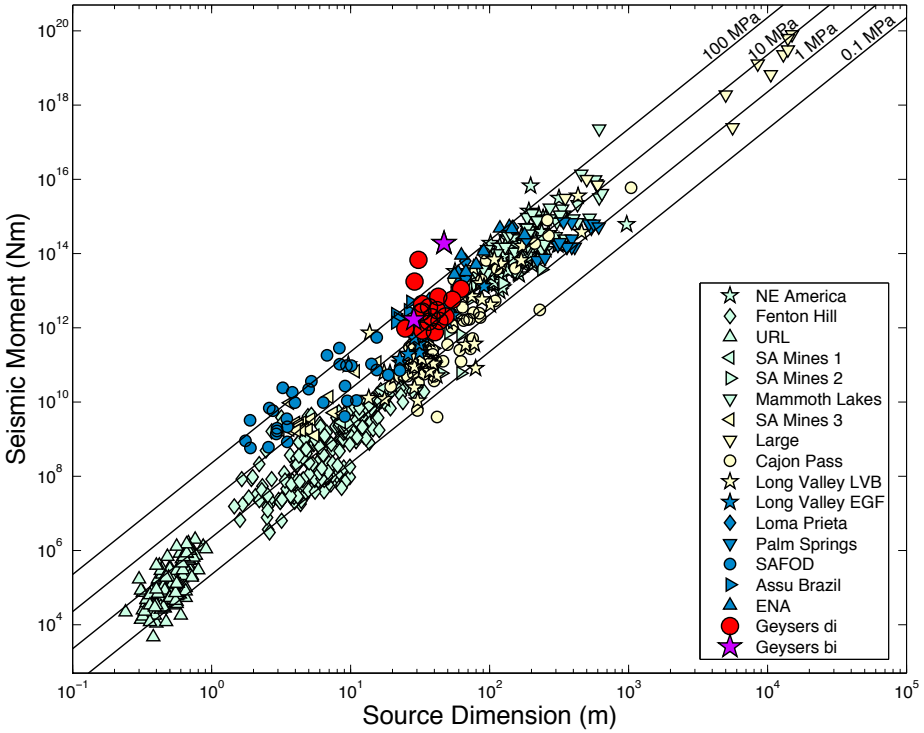

Figure 5. Global compilation of seismic moment versus source radius color coded by used method or data type. Blue indicates EGF methods, light pink indicates slip inversion methods or deep borehole data, and light blue indicates individual fitting methods. This study results are shown in purple and red, using purple starts for before injection (bi) and red circles for during injection (di) micro-earthquakes. The diagonal lines indicate constant stress drop. (After Tomic *et al.*, 2009, adapted from Abercrombie and Leary, 1993). Data points are: NE America (Boatwright 1994), Fenton Hill (Fehler & Phillips, 1991), URL (Gibowicz *et al.*, 1991), S. A Mines 1 (McGarr *et al.*, 1990), S. A Mines 2 (Spottiswoode and McGarr, 1975), Mammoth Lakes (Archuleta *et al.*, 1982), S. A. Mines 3 (Yamada *et al.*, 2007), Large (compilation of Abercrombie and Rice, 2005, Table 5: Dreger and Helmberger 1991, Mori 1996, Hough and Dreger 1995, Ji *et al.* 2002, Venkataraman *et al.* 2000, Wald 1995, Wald and Heaton 1994, Wald *et al.* 1996, Wald *et al.* 1991), Cajon Pass (Abercrombie, 1995), Long Valley (Ide *et al.*, 2003, individual and EGF studies), Loma Prieta (Hough *et al.*, 1991), Palm Springs (Mori and Frankel 1990), SAFOD (Imanishi and Ellsworth, 2006), Açu Brazil (Tomic *et al.*, 2009), ENA (Xie *et al.*, 1991; Li *et al.*, 1995; Shi *et al.*, 1998), Geysers (this study).

Conclusions and Future Work

We investigate the source parameters of micro-earthquakes at the Northwest Geysers, looking for temporal and spatial variations. We also investigate changes in the source parameters of micro-earthquakes near injection well Prati 9, before and during water injection begins. Our results indicate that micro-earthquakes at the Northwest Geysers have on average small radius and large stress drops. The stress drops are within the range but slightly higher than natural occurring tectonic micro-earthquakes. Possible explanations for the high stress drop are, for example, the high crustal temperatures and presence of fluids, which may re-strengthen the faults by accelerating the fault healing rates through chemical processes; and the fracturing of intact rock induced by the injection cold water. The higher stress drop values of the larger mictro-earthquakes may be a consequence of an higher uncertainty in the source parameters estimates of these micro-earthquakes. We observed that the micro-earthquakes which occurred after water injection were slightly deeper (by ~1 km) than those that occurred prior to injection, but we do not see a clear increase in stress drops. As we proceed with our study and include more micro-earthquake source parameter estimates into our results, a better assessment of time and space variation will be available.

The important result of this study is that stress drops of shallow (<3.5 km) micro-earthquakes at the Northwest Geysers, both naturally occurring and injection induced, are as large or larger than the stress drops of naturally occurring tectonic earthquakes. This source information has implications for understanding the physics of faulting and for seismic potential assessment in areas of ongoing geothermal exploration.

References

Abercrombie, R. E. (1995). Earthquake source scaling relationships from -1 to 5 ML using seismograms recorded at 2.5 km depth, *J. Geophys. Res.*, 100, 24015-24036.

Abercrombie, R. E., and J. R. Rice (2005). Small earthquake scaling revisited: can it constrain slip weakening? *Geophys. J. Int.*, 162, 406-424.

Abercrombie, R. E., and P. C. Leary (1993). Source parameters of small earthquakes recorded at 2.5 km depth, Cajon Pass, southern California: implications for earthquake scaling, *Geophys. Res. Lett.*, 20, 1511-1514.

Archuleta, R. J., E. Cranswick, C. Mueller, and P. Spudich (1982). Source parameters of the 1980 Mammoth Lakes, California, earthquake sequence, *J. Geophys. Res.,* 87(B6), 4595–4607.

Boatwright, J. (1994). Regional propagation characteristics and source parameters of earthquakes in Eastern North America, *Bull. Seism. Soc. Am.*, 84, 1-15.

Boatwright, J., and J. B. Fletcher (1984). The partition of radiated energy between *P* and *S* waves, *Bull. Seism. Soc. Am.*, 74, 361-376.

Bonner, B., L. J. Hutchings, and P. Kasameyer (2006). A strategy for interpretation of microearthquake tomography results in the Salton Sea Geothermal Field based upon rock physics interpretations of State 2-14 borehole logs, *Geothermal Resource Council Annual Meeting, San Diego, California, September 2006*,UCRL-PROC-222141.

Brune, J. (1970). Tectonic stress and the spectra of seismic shear waves from earthquakes, *J. Geophys. Res.*, 75, 4997-5009.

Caceci, M.S., and W.P. Cacheris (1984) *Numerical Recipes,* 1998, Chapter 10.4.

Console, R., and R. Rosini (1998). Non-double-couple microearthquakes in the geothermal field of Larderello, central Italy, *Tectonophysics*, 289, 203–220.

Eberhart-Phillips, D., and D. H. Oppenheimer (1986). Induced Seismicity in The Geysers Geothermal Area, California, *J. Geophys. Res.*, 91, 11463-11476.

Eshelby, J. D. (1957). The determination of the elastic field of an ellipsoidal inclusion and related problems, *Proc. Roy. Soc. Lond., A*, 241, 376-396.

Fehler, M., and W. S. Phillips (1991). Simultaneous inversion for *Q* and source parameters of microearthquakes accompanying hydraulic fracturing in granitic rock, *Bull. Seism. Soc. Am,* 81**,** 553-575.

Gibowicz, S. J., R. P Young, S. Talebi and D. J. Rawlence (1991). Source parameters of seismic events at the Underground Research Laboratory in Manitoba, Canada: scaling relations for events with moment magnitude smaller than -2, *Bull. Seism. Soc. Am.,* 81**,** 1157-1182.

Gok, R., L. Hutchings, K. Mayeda and D. Kalafat (2009). Source parameters for 1999 North Anatolian fault zone aftershocks. *Pure and Applied Geophysics*, 166, 547-566.

Hanks, T., and H. Kanamori (1979). A moment magnitude scale, *J. Geophys. Res.*, 84, 2348-2350.

Hough, S.E., J. M. Lees, and J. Monastero (1999). Attenuation and Source Properties at the Coso Geothermal Area, California, *Bull. Seism. Soc. Am*, 89(6), 1606-1619.

Hough, S.E., L. Seeber, A Lerner-Lam, J.G. Armbruster, and H. Guo (1991). Empirical Green's function analysis of Loma Prieta aftershocks, *Bull. Seism. Soc. Am*, 81, 1737-1753.

Hutchings, L. (2002). Program NetMoment, a Simultaneous Inversion for Moment, Source Corner Frequency, and Site Specific t*. Lawrence Livermore National Laboratory, UCRL-ID 135693.

Hutchings, L., and F. Wu (1990). Empirical Green's functions from small earthquakes – A waveform study of locally recorded aftershocks of the San Fernando earthquake, *J. Geophys. Res.*, 95, 1187-1214.

Ide, S., and G. C. Beroza (2001). Does apparent stress vary with earthquake size? *Geophys. Res. Lett.*, 28, 3349-3352.

Ide, S., G. C. Beroza, S. G. Prejean and W. L. Ellsworth (2003). Apparent break in earthquake scaling due to path and site effects on deep borehole recordings, *J. Geophys. Res.*, 108, doi:10.1029/2001JB001617.

Imanishi, K., and W. L. Ellsworth (2006). Source scaling relationships of microearthquakes at Parkfield, CA, determined using the SAFOD pilot hole seismic array, in *Earthquakes: Radiated Energy and the Physics of Faulting, Geophys. Monogr. Ser.*, vol. 170, edited by R.E. Abercrombie, A. McGarr, H. Kanamori and G. Di Toro, pp. 81–90, American Geophysical Union, Washington, D.C.

Kanamori, H. (1994). Mechanics of Earthquakes, *Ann. Rev. Earth & Planetary Sciences*, 22, 207-237.

Karner, S. L. (2005). Stimulation techniques used in enhanced geothermal systems: perspectives from geomechanics and rock physics, *Proceedings, 30th Workshop on Geothermal Reservoir Engineering*, Stanford University, Stanford, CA, SGP-TR-176.

Lama, R. D., and V. S. Vutukuri (1978). *Handbook on Mechanical Properties of Rocks*, Volume II: Testing Techniques and Results, Clausthal, Germany, Trans. Tech. Publications, 1978, 245 pp., (J. Phys. Earth. 42, 377–397).

Li, Y., C. Jr. Doll, and M. N. Toksöz (1995). Source characterization and fault plane determination for M_{bLg} = 1.2 to 4.4 earthquakes in the Charlevoix Seismic Zone, Quebec, Canada, *Bull. Seism. Soc. Am.*, 85, 1604-1621.

Madariaga, R. (1976). Dynamics of an expanding circular crack, *Bull. Seism. Soc. Am.*, 66, 639-666.

Majer, E.L, R. Baria , M. Stark, S. Oates, J. Bommer, B. Smith and H. Asanuma (2007b). Induced seismicity associated with Enhanced Geothermal Systems, *Geothermics*, 36, 185-227.

Majer, L. E., and J. E. Peterson (2007a). The impact of injection on seismicity at The Geysers, California Geothermal Field, *Int. J. Rock Mech. Mining Sci.*, 44, 1079-1090.

McGarr, A. (1999). On relating apparent stress to the stress causing earthquake fault slip, *J. Geophys. Res.*, 104, 3003-3001.

Miller, A. D., B. R. Julian and G. R. Foulger (1998). Three-dimensional structure and moment tensors of non-double-couple earthquakes at the Hengill-Grensdalur volcanic complex, Iceland, *Geophys. J. Int.*, 133, 309-325.

Mori, J. J., and A. Frankel (1990). Source parameters for small events associated with the 1986 North Palm Springs, California, earthquake determined using empirical Green functions, *Bull. Seism. Soc. Am.*, 80, 278-295.

Nelder, J. A., and R. Mead, (1965). A simplex method for function minimization, *Computer J.*, 7, 308.

Park, J., C. R. Lindberg, and F. L. Vernon III (1987). Multitaper spectral analysis of high-frequency seismograms, *J. Geophys. Res.*, 92, 12675-12684.

Prieto, G. A., R. L. Parker, and F. L. Vernon (2009). A Fortran 90 library for multitaper spectrum analysis, *Computers and Geosciences*, doi:10.1016/j.cageo.2008.06.007.

Romero, A. E., Jr., T. McEvilly and E. L. Majer (1997). 3-D Microearthquake Attenuation Tomography at the Northwest Geysers Geothermal Region, California, *Geophysics*, 62(1), 149-167.

Shi, J., W.-Y. Kim, and P. Richards (1998). The corner frequency and stress drops of intraplate earthquakes in the northeastern United States, *Bull. Seism. Soc. Am.*, 88, 531-542.

Smith, J. L. B., J. J. Beall, and M. A. Stark (2000). Induced seismicity in the SE Geysers field, *Geothermal Resources Council Trans.*, 24, 24-27.

Sonley, E., and R. E. Abercrombie (2006). Effects of methods of attenuation correction on source parameter determination, *in Earthquakes: Radiated Energy and the Physics of Faulting, Geophys. Monogr. Ser.*, vol. 170, edited by R.E. Abercrombie, A. McGarr, H. Kanamori and G. Di Toro, pp. 91-97, American Geophysical Union, Washington, D.C.

Spottiswoode, S. M., and A. McGarr (1975). Source parameters of tremors in a deep level gold mine, *Bull. seism. Soc. Am.* 65, 93-112.

Street, R. L., R. B. Herrmann and O. W. Nuttli (1975). Spectral characteristics of the Lg wave generated by central United States earthquakes, *Geophysical Journal of the Royal Astronomical Society* 41**,** 51-63.

Taggart, J., S. Ohlendorf, S. Ford, P. Hellweg and D. Dreger, (2009). Anomalous Moment Tensor Solutions for The Geysers, CA, *2008-2209 Annual report of the Berkeley Seismological Laboratory*, http://seismo.berkeley.edu/annual_report/ar08_09/node17.html#taggart09_1_1.

Thomson, D. J. (1982). Spectrum estimation and harmonic analysis. *Proceedings of the IEEE*, 70, 1055-1096.

Tomic, J., R. E. Abercrombie and A. F. do Nascimento (2009). Source parameters and rupture velocity of small M≤2.1 reservoir induced earthquakes, *Geophys. J. Int.*, doi:10.1111/j.1365-246X.2009.04233.x.

Viegas, G., R. E. Abercrombie and W.-Y. Kim (2010). The 2002 M5 Au Sable Forks, NY, earthquake sequence: source scaling relationships and energy budget, *J. Geophys. Res.* (in press).

Xie, J., Z. Liu, R. B. Hermmann, and E. Cranswick (1991). Source processes of three aftershocks of the 1983 Goodnow, New York, earthquake: High-resolution images of small, symmetric ruptures, *Bull. Seism. Soc. Am.*, 81, 818-843.

Yamada, T., J. J. Mori, S. Ide, R. E. Abercrombie, H. Kawakata, M. Nakatani, Y. Iio, and H. Ogasawara (2007). Stress drops and radiated seismic energies of microearthquakes in a South African gold mine, *J. Geophys. Res.*, 112, B03305, doi:10.1029/2006JB004553.